Simulating Hurricane Storm Surge in the Lower Mississippi River under Varying Flow Conditions

R. C. Martyr, M.ASCE[1]; J. C. Dietrich[2]; J. J. Westerink, M.ASCE[3]; P. C. Kerr[4]; C. Dawson[5]; J. M. Smith, M.ASCE[6]; H. Pourtaheri[7]; N. Powell, D.WRE, M.ASCE[8]; M. Van Ledden[9]; S. Tanaka[10]; H. J. Roberts[11]; H. J. Westerink[12]; and L. G. Westerink[13]

Abstract: Hurricanes in southeastern Louisiana develop significant surges within the lower Mississippi River. Storms with strong sustained easterly winds push water into shallow Breton Sound, overtop the river's east bank south of Pointe à la Hache, Louisiana, penetrate into the river, and are confined by levees on the west bank. The main channel's width and depth allow surge to propagate rapidly and efficiently up river. This work refines the high-resolution, unstructured mesh, wave current Simulating Waves Nearshore + Advanced Circulation (SWAN + ADCIRC) SL16 model to simulate river flow and hurricane-driven surge within the Mississippi River. A river velocity regime–based variation in bottom friction and a temporally variable riverine flow-driven radiation boundary condition are essential to accurately model these processes for high and/or time-varying flows. The coupled modeling system is validated for riverine flow stage relationships, flow distributions within the distributary systems, tides, and Hurricane Gustav (2008) riverine surges. **DOI: 10.1061/(ASCE)HY.1943-7900.0000699.** © *2013 American Society of Civil Engineers.*

CE Database subject headings: Storm surges; Mississippi River; Hurricanes; Rivers and streams; Hydrodynamics; Numerical models; Simulation.

Author keywords: Storm surge; Mississippi River; Hurricanes; Rivers; Hydrodynamics; Numerical models; Storm surge generation; Propagation and attenuation.

Introduction

The central Gulf coast's geographical features and location make it particularly vulnerable to large storm surge during hurricanes. Southeast Louisiana is defined by low-lying topography, with many floodplains, marshes, and interconnected lakes (Fig. 1). The Mississippi River meanders through the region, and its southern reach is surrounded by shallow bays and lakes, such as Lake Borgne, and shallow open waters to the east. The river's delta protrudes to the edge of the continental shelf and contains many distributaries and interconnected fresh-water and brackish marshes. The city of New Orleans is bounded by Lake Pontchartrain to the north and the river to the south. Plaquemines Parish, the southern boundary of the state, encompasses the southern portion of the river and its delta, which are also surrounded by extensive marshes and sounds, such as Caernarvon Marsh and Chandeleur and Breton sounds to the east, and Barataria Bay to the west. These features define the geography of the region and are interconnected to the Gulf by the river, natural and artificial channels, and the low-lying floodplain.

Periodic flooding and navigational demands prompted levee development along the river. These levees extend downriver to Pointe à la Hache, Louisiana, on the east river bank, and continue further southward to Venice, Louisiana, on the west bank. Due to the regional geography, hurricane storm surge is effectively captured by the western river levee. Hurricanes, such as Betsy (1965), Katrina (2005), and Gustav (2008), pushed surge from the southeast and east into Breton Sound and flooded the narrow marsh and eastern river banks of lower Plaquemines Parish, Louisiana (Westerink et al. 2008; Bunya et al. 2010; Dietrich et al. 2010, 2012). The western levees that extend 60 km farther south along the river enable an efficient buildup of surge. The river's width and depth facilitate the propagation of this surge upriver to New Orleans and Baton Rouge, Louisiana.

The Mississippi River experiences interannual and intra-annual variations in flow due to many factors including seasonal

[1]Dept. of Civil and Environmental Engineering and Earth Sciences, Univ. of Notre Dame, Notre Dame, IN 46556 (corresponding author). E-mail: rmartyr@nd.edu

[2]Institute for Computational Engineering and Sciences, Univ. of Texas, Austin TX 78712.

[3]Dept. of Civil and Environmental Engineering and Earth Sciences, Univ. of Notre Dame, Notre Dame, IN 46556.

[4]Dept. of Civil and Environmental Engineering and Earth Sciences, Univ. of Notre Dame, Notre Dame, IN 46556.

[5]Institute for Computational Engineering and Sciences, Univ. of Texas, Austin TX 78712.

[6]Coastal Hydraulics Laboratory, U.S. Army Engineer Research and Development Center, Vicksburg, MS 39180.

[7]New Orleans District, U.S. Army Corps of Engineers, New Orleans, LA 70118.

[8]New Orleans District, U.S. Army Corps of Engineers, New Orleans, LA 70118.

[9]Haskoning Nederland B.V., Rotterdam, The Netherlands.

[10]Earthquake Research Institute, Univ. of Tokyo, Tokyo 113-0032, Japan.

[11]ARCADIS INC., Boulder, CO 80301.

[12]Dept. of Civil and Environmental Engineering and Earth Sciences, Univ. of Notre Dame, Notre Dame, IN 46556.

[13]Dept. of Civil and Environmental Engineering and Earth Sciences, Univ. of Notre Dame, Notre Dame, IN 46556.

Note. This manuscript was submitted on December 6, 2011; approved on November 2, 2012; published online on November 5, 2012. Discussion period open until October 1, 2013; separate discussions must be submitted for individual papers. This paper is part of the ***Journal of Hydraulic Engineering***, Vol. 139, No. 5, May 1, 2013. © ASCE, ISSN 0733-9429/2013/5-492-501/$25.00.

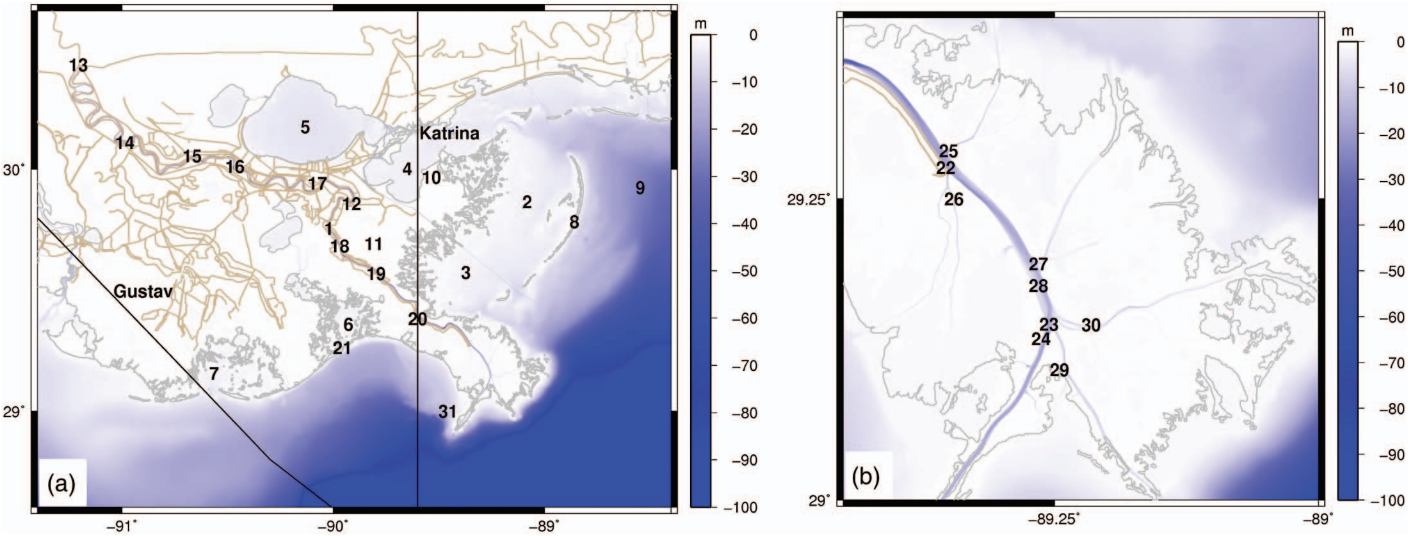

Fig. 1. (Color) (a) Schematic of southeastern Louisiana and (b) the Mississippi River Delta with bathymetry shown in meters; solid lines indicate Gustav's and Katrina's tracks (black); geographic locations of interest are indicated by the numbers designated in the appendix

effects (such as snowmelt, rainfall, and Gulf-wide upper-layer temperature-induced expansion and contraction), tidal variations, regional and Gulf-wide wind patterns, inflow from river tributaries, and climatological variations (Walker et al. 2005; Sanchez-Rubio et al. 2011). Intraannual flow variations along the Mississippi River typically generate lower flows during hurricane (June to November) and peak-hurricane (August to October) seasons than during spring months (www.mvn.usace.army.mil/eng/edhd/wcontrol/miss.asp). This decrease in flows during hurricane season does not imply that riverine flows are always low or steady during that period. During Hurricane Katrina, which made landfall on August 29, 2005, river flow was exceptionally low at 4,800 $m^3 s^{-1}$, approximately 3,000 $m^3 s^{-1}$ below the average peak hurricane-season flow. In contrast, during hurricanes Gustav and Ike in September 2008, the river discharge ranged from 8,000 to 14,160 $m^3 s^{-1}$, higher than the peak hurricane-season average. Thus, it is expected that a hurricane can occur during a range of riverine discharges from low to high. Moreover, flow in the Mississippi River was fairly constant during and after Katrina, but increased more than 4,000 $m^3 s^{-1}$ in the week between Gustav and Ike, causing high flow variation in a short duration. As many metropolitan areas along the Mississippi River face risk both from riverine flooding and hurricane surge, it is important to accurately model the effects of high and variable riverine flows on hurricane surge and overall water levels during a hurricane event.

Highly detailed, unstructured mesh, computational models of southern Louisiana have been developed to resolve complex physical processes at the basin, shelf, floodplain, and channel scales (Westerink et al. 2008). These unstructured meshes have high levels of resolution, varying from kilometers in the deep ocean to tens of meters in the nearshore zone. The Advanced Circulation (ADCIRC) coastal circulation and storm surge model has been coupled to various wave models and validated with river stages, tides, and hurricane-driven waves and surge throughout southern Louisiana and the Gulf (Bunya et al. 2010; Dietrich et al. 2010, 2011a, b, 2012).

In this paper, river velocity regime-based variations in bottom stress are implemented in order to parameterize the effects of ripples and dunes from low to high flows. Furthermore, the large variability in riverine flow during hurricane events, such as that seen in Hurricane Gustav, has prompted the development of a temporally varying riverine flow-driven radiation boundary condition in the ADCIRC model. The improved Simulating Waves Nearshore (SWAN)+ADCIRC model using these two new features in combination with the SL16 mesh are validated for riverine stages between Baton Rouge, Louisiana, and Venice, Louisiana, and flow distribution through the river's distributaries. U.S. Army Corps of Engineers (USACE) water level observations and model results are compared at six gauges along the Mississippi River for flows ranging between 4,500 and 32,000 $m^3 s^{-1}$. Flows through seven deltaic channels are described as ratios of the main channel flow to provide insight into the distribution of flow through the delta. The model enhancements improve model performance when compared to previous model validations [e.g., Bunya et al. (2010)]. Validation of Hurricane Gustav (2008) is also presented, with special focus on water elevations within the Mississippi River. The time-varying riverine flows are applied for this simulation based on daily-specified USACE measured riverine flows at Tarbert Landing, Mississippi. Relative to previous hindcasts [e.g., Dietrich et al. 2011a), the time-varying flow riverine radiation boundary performs better when model results are compared to National Oceanic and Atmospheric Administration (NOAA) and USACE river gauge observations.

SL16 Wave-Current Modeling System

ADCIRC Model and the River Radiation Boundary Condition

ADCIRC-2DDI, the depth-integrated version of the ADCIRC coastal ocean model, simulates the evolution of water elevations and currents using a modified form of the shallow-water equations and a continuous Galerkin–based finite-element solution (Luettich and Westerink 2004; Atkinson et al. 2004a, b; Dawson et al. 2006; Kubatko et al. 2009; Tanaka et al. 2011). Riverine, tidal, and hurricane-driven flows on continental shelves and in inland waters are well described by depth-averaged flows due to the processes themselves and/or the energetic wave-induced vertical mixing during hurricanes. ADCIRC's unstructured meshes allow highly localized mesh resolution in areas in which system and response gradients are large and in regions of particular interest. High scalability up to tens of thousands of computational cores permits comprehensive domains that are highly resolved (Tanaka et al. 2011; Dietrich et al. 2012).

ADCIRC implements a variety of boundary types and conditions, including land, riverine flow, and surface water elevation boundary conditions. Tides for U.S. East and Gulf coast ADCIRC models are typically forced at the Atlantic 60°W open-ocean boundary and within the domain by tidal potential forcing functions. The K_1, O_1, Q_1, K_2, M_2, N_2, and S_2 tidal constituents are forced using results from Le Provost's (FES95.2) global tidal model and the P_1 constituent from the Oregon State University Tidal Inversion Software (Le Provost et al. 1998; Mukai et al. 2001; Egbert and Erofeeva 2002).

At river boundaries, ADCIRC uses a river wave radiation boundary condition to specify a river flow into the domain while allowing the propagation of long waves (due mainly to tides and storm surge) out of the domain, thus preventing the reflection of these long waves at the boundary (Westerink et al. 2008). The river radiation boundary condition linearly parses the normal flow at the boundary into two components: one component represents the contribution due to the river flow, q_{river}, while the other represents the contribution due to propagating long waves, including tides and storm surge, q_{wave}.

$$q_N(t) = -q_{\text{river}} + q_{\text{wave}}(t)$$

By defining a wave speed, c, and the water elevation due to all flows, $\zeta(t)$, the river radiation boundary condition can be expressed as

$$q_N(t) = -q_{\text{river}} + c(\zeta(t) - \zeta_{\text{river}})$$

and is used to evaluate the total normal flow at the river boundary due to all flows. If it is assumed that the river component of flow, q_{river}, is constant in time, then the corresponding stage for that flow rate, ζ_{river}, must be evaluated by (1) ramping up the model from a cold start; (2) applying only the river flow, q_{river}, as a spatially varying but temporally constant flux-specified boundary condition; (3) using a half-day hyperbolic tangent ramp function; and (4) then allowing the river stages to come to equilibrium for this river flow. Steady-state equilibrium requires 2 to 5 days, at which time the nodal stage values on the river boundary are saved as ζ_{river}. Then the tidal, wind, atmospheric pressure, and wind wave forcing functions can be initiated, and the river radiation boundary condition is applied by using the specified values of q_{river}, the associated stage ζ_{river}, and the values of the water surface elevation at river boundary nodes, $\zeta(t)$. This river radiation boundary condition allows tides and storm surge to pass through a boundary for any temporally constant river flow.

In this paper, a spatially and temporally varying riverine flow-driven radiation boundary condition is implemented. The new total normal flow can be described as

$$q_N(t) = -q_{\text{river}}(t) + c(\zeta(t) - \zeta_{\text{river}}(t))$$

where $q_{\text{river}}(t)$ and $\zeta_{\text{river}}(t)$ = functions of time. The cold start procedure described for the temporally constant river flows is still used to initiate the computation. However, once the river has reached its initial equilibrium for a selected initial river flow, the radiation boundary condition is applied using temporally variable river flow values, $q_{\text{river}}(t)$, and the associated dynamically correct stage, $\zeta_{\text{river}}(t)$, at the river boundary (assuming no forcing mechanisms other than river flow). The best way to accomplish this is to establish an a priori river flow stage relationship over a range of riverine flows, as described in "Mississippi River Flow Validation." With this precomputed stage flow curve at the boundary, the time-varying implementation of the river radiation boundary condition can be implemented, and all other forcing functions such as tides, winds, atmospheric pressure, and wind waves can be initiated. Using the precomputed flow stage curve does assume that the rate of change of the river flows is slow enough that the precomputed flow stage curves remain a good estimate for the surface water elevation response. The method maintains the radiative capabilities of the previously implemented river radiation boundary condition (Westerink et al. 2008) while allowing the river-only flow and associated river-only elevation to vary in time.

SWAN Wave Model

Interaction of ocean circulation and wind waves is critical in simulating hurricanes due to the effect of water levels and currents on wave propagation and dissipation, and the effect of wave transformation, wind wave–induced vertical mixing, and wave-modified bottom friction on circulation. Wave transformation generates radiation stress gradients that can increase water levels by as much as 20% on broad continental shelves and 35% in steep sloped regions (Resio and Westerink 2008; Dietrich et al. 2010).

The SWAN model is a third-generation, phase-averaged wave model used for the simulation of waves in shallow, intermediate, and deep waters (www.swan.tudelft.nl) (Booij et al. 1999; Ris and Holthuijsen 1999). Recent development of an unstructured version of SWAN has allowed for tight coupling of this wave model with ADCIRC, resulting in the SWAN + ADCIRC wave-circulation model (Zijlema 2010; Dietrich et al. 2011b, 2012). SWAN uses ADCIRC-generated water levels and currents to determine wave refraction and shoaling and depth-induced breaking, and ADCIRC uses SWAN-generated wave radiation stress gradients as additional forcing in solving for water levels and currents.

Unstructured Mesh Development

Domain, Bathymetry, Topography, and Resolution

The SL16 domain includes the western North Atlantic Ocean, the Gulf of Mexico, and the Caribbean Sea, with an eastern boundary along the 60°W meridian. Bathymetry and topography for SL16, with details in southeastern Louisiana shown in Figs. 2(a and b), is assigned using available NOAA and USACE bathymetric databases. Inland topography is obtained from light detection and ranging (LIDAR) databases (atlas.lsu.edu/lidar, /lidar.cr.usgs.gov). Marsh topography is based on USGS Louisiana GAP Analysis land use maps, with topographical height correlations for a variety of marsh types. Levee and road heights are assigned from USACE surveys and/or LIDAR databases. Details of the mesh development are in Dietrich et al. (2011a).

The SL16 mesh contains high levels of localized resolution, with 5,069,208 vertices and 10,017,091 triangular elements. Resolution is highly concentrated in southern Louisiana, with 63% of the mesh's vertices located in 1% of the mesh's geographic space. Resolution in the Gulf of Mexico ranges from 4–6 km, and, as shown in Figs. 2(c and d), increases on the continental shelf to 500–1,000 m. Smaller mesh spacing of 30–150 m is placed within the Mississippi River, its delta, and its distributaries for improved riverine and tidal flow, as well as hurricane surge penetration and propagation. The river and delta portion of the mesh totals 1.5 million vertices (or 30% of the full mesh). This is a significant increase in resolution from previously published models [for example, the SL15 model used in Bunya et al. (2010)], which placed 100–150 m nodal spacing within the river, the delta, and surrounding wetlands. The SL16 model refines the depiction of river bathymetry and batture topography and has a much higher resolution and more accurate topographic representation of the

J. Hydraul. Eng. 2013.139:492-501.

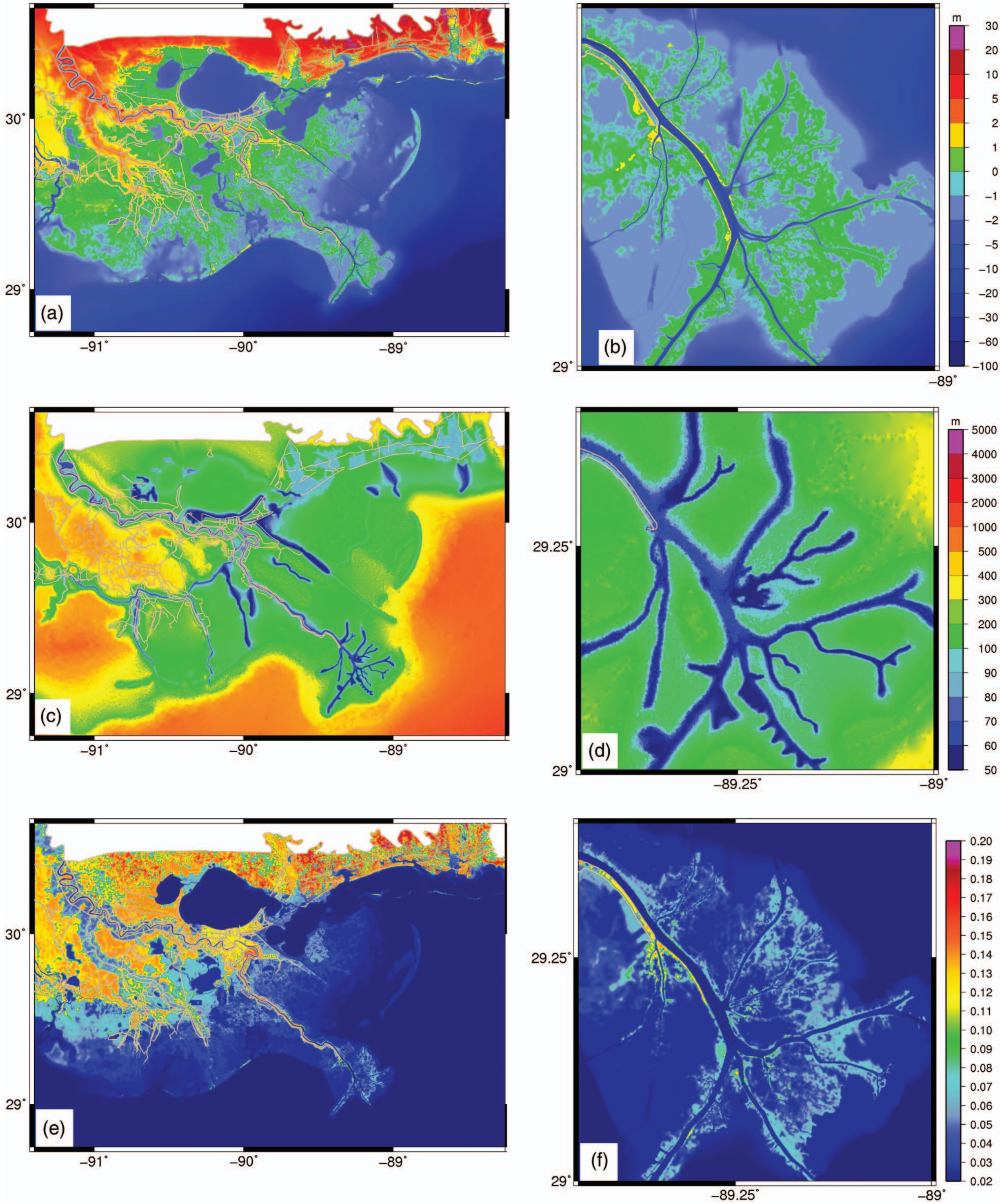

Fig. 2. (Color) (a) Bathymetry/topography, (c) mesh resolution in terms of nodal spacing, and (e) Manning's n values of southeastern Louisiana; (b) Bathymetry/topography, (d) mesh resolution in terms of nodal spacing, and (f) Manning's n values of the lower Mississippi River delta birds foot and distributaries

wetland systems in and around the river, as compared to previous models (Dietrich et al. 2011a).

The Mississippi River has three main distributaries, namely South Pass, Southwest Pass, and Pass à Loutre, which exit directly into the Gulf of Mexico. Several other passes feed the surrounding marshes. These outlets include Baptiste Collette Bayou, Grand Pass, Main Pass, and Cubit's Gap [Fig. 1(b)]. These channels convey thousands of cubic meters of water, but are narrow in cross section. In addition, there are many openings south of Pointe à la Hache, Louisiana, allowing continuous lateral discharge to the surrounding marshes and sounds. Previous models such as the SL15 model (Bunya et al. 2010) include only a moderate resolution definition of some of these passes. The SL16 model improvements lead to better flow stage relationships in the upper river

J. Hydraul. Eng. 2013.139:492-501.

and flow distribution in the distributaries as compared to the SL15 model.

Vertical Datum and Steric Water Level Adjustments

Water levels at the beginning of ADCIRC simulations are adjusted to account for the vertical datum, as well as seasonal variability in sea levels in the Gulf of Mexico. Simulations are referenced to the North American Vertical Datum of 1988 updated to the 2004.65 epoch, NAVD88 (2004.65), by increasing water levels by 0.134 m at the beginning of the simulation (Bunya et al. 2010). In addition, an adjustment is needed due to the seasonal variability of the local mean sea level (LMSL) in the Gulf, caused by factors such as upper Gulf thermal expansion, riverine fresh water outflows, and regional and local winds. NOAA long-term stations at Dauphin Island, Alabama, Eugene Island, Louisiana, and Grand Isle, Louisiana, indicate an average surface elevation increase of 0.036 m in August and 0.127 m in September as compared with the annual mean sea level (tidesandcurrents.noaa.gov/sltrends/sltrends.html). Thus, for Hurricane Gustav, a total adjustment of $0.134 + 0.086 = 0.22$ m is used, where the first number is the datum adjustment and the second number is the interpolated-in-time steric adjustment.

Hydraulic Friction and Eddy Viscosity

Bottom friction is computed using a quadratic parameterization of bottom stress with a Manning's n formulation (Dietrich et al. 2011a). Nodal-based Manning's n coefficients for land are spatially assigned using land cover information from the USGS Louisiana and Mississippi GAP Analysis (LA-GAP, MS-GAP) Programs, NOAA's regional Coastal Change Analysis Program (C-CAP), and the USGS National Land Cover Database (NLCD) in Texas and Alabama.

The spatial representation of Manning's n coefficients was specified for all water bodies by correlating values to the bottom surface characteristics (Dietrich et al. 2011a). Recent USGS data on the sediment of the Gulf Coast shelves and seafloor (Buczkowski et al. 2006) indicate a muddy composition on the Louisiana–Texas shelf (and a value of 0.012 is specified), and a sandy composition on the Florida shelf (and a value of 0.022 is specified). Shorelines tend to be sandier and rougher even in cases in which lake and shelf bottoms are muddy, thus Manning's n values vary between a value of 0.025 at the zero meter contour to the local shelf value (0.012 on the Louisiana–Texas shelf and 0.022 on the Florida shelf) at depths of 5 m and greater. The deep ocean for depths greater than or equal to 200 m is assigned to 0.012. The shelf friction values specified are a major refinement in the SL16 model when compared with previous models (Bunya et al. 2010, Dietrich et al. 2012). The Mississippi River is assigned a base Manning's n value of 0.022; in areas of significant meandering, such as the region from Baton Rouge, Louisiana, to English Turn, Louisiana, Manning's n values are increased to 0.025 based on a meandering ratio adjustment from Chow (1959). Shallow meandering channels in the mesh are assigned 0.035.

Riverine frictional resistance is affected by the material composition of the channel, bedforms, the presence of vegetation and other obstructions, channel shape, and meandering. The presence of bedforms increases frictional resistance during low river velocities, and through their degradation at high velocities experienced in upper flow regime conditions (typically above 1.5 m/s) decreases resistance (Arcement and Schneider 1989; Van Rijn 2007; Warner et al. 2008). A velocity regime–based linear variation in Manning's n values in the Mississippi River is applied. Low flow values are constant up to depth-averaged river velocities of 1.5 m/s, decrease linearly between 1.5 and 2.0 m/s, and have a defined lower limit equal to 85% of the river's low flow Manning's n values at velocities above 2.0 m/s. Lateral eddy viscosity is set uniformly in all open water to 2 $m^2 s^{-1}$ and to 20 $m^2 s^{-1}$ in marshes and over land.

Mississippi River Flow Validation

Stage Discharge Relationships

Riverine validation in the SL16 model is performed by comparing measured and ADCIRC-predicted water elevations along the Mississippi River at USACE water level stations from Baton Rouge, Louisiana, to Venice, Louisiana (Fig. 3). The USACE has measured stage discharge data at each station, where daily water elevations are matched with the time-lagged flow rate from the Tarbert Landing, Mississippi, flow measurement transect. Using data from several years, a best-fit stage flow curve can be obtained for each station. Station water level data in Fig. 3 vary on average between 12 and 22 cm from the best-fit curves at these stations (Table 1). This variability is related to intraannual Gulf mean sea level trends, tides, wind-driven and frontal events including hurricanes, and various processes that cause hysteresis in the river water level response. Intraannual Gulf mean water levels tend to be

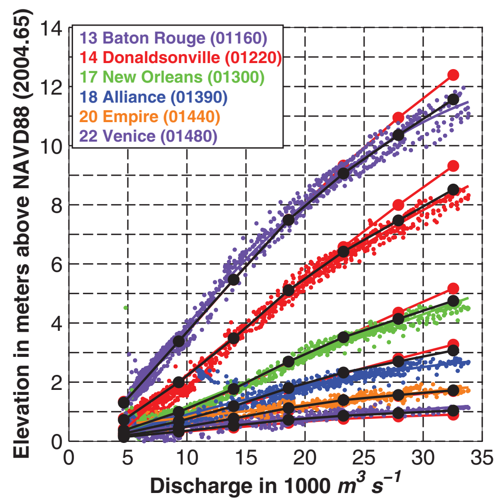

Fig. 3. (Color) Flow stage relationship for six USACE-maintained water level gauges along the Mississippi River; measurement data are indicated with the colored points and the best-fit curves to the data at each station are shown in solid colored lines; ADCIRC SL16 model results using a Manning's n formulation without regime dependence are denoted by red dots connected by red lines; ADCIRC SL16 model results using regime-based friction are denoted by black dots connected by black lines

Table 1. Summary of Error Statistics for River Flow Stage at Six Mississippi River Water Level Measurement Stations

Gauge number/name	Data years	$E_{\text{meas.-bf}}$ (m)	E_{SL16NR} (m)	E_{SL16R} (m)
13 Baton Rouge, Louisiana	1991, 1997, 2005	0.2235	0.3852	0.1462
14 Donaldsonville, Louisiana	1991, 1997, 2005	0.2054	0.3719	0.1564
16 New Orleans	1991, 1997, 2005	0.1558	0.2073	0.1161
18 Alliance	1991, 1997, 2007	0.1931	0.2317	0.1874
20 Empire, Louisiana	1991, 1997, 2003	0.1188	0.1732	0.1489
22 Venice, Louisiana	1997, 2005	0.1274	0.1630	0.0927

Note: $E_{\text{meas.-bf}}$ is the average absolute difference between USACE-measured data and the measurement data-derived best-fit curves. $E_{\text{model-bf}}$ shows the average absolute difference between the SL16 model results without and with the flow regime–based Manning's n (SL16NR and SL16R, respectively) and the data-derived best-fit curves.

J. Hydraul. Eng. 2013.139:492-501.

biharmonic in the northern Gulf with water levels being the lowest in January, followed by a late spring peak in May, a lowering through July, and a subsequent September high. The process is driven by a combination of Gulf upper water layer expansion due to temperature, Mississippi and Atchafalaya River fresh water lenses, and seasonal winds, and has an associated amplitude range of 12 cm below and 15 cm above LMSL. In lower reaches of the river, tidal amplitude ranges of 10–35 cm enter the river mouth and can propagate upstream past New Orleans. Hysteresis-based variability in flow stage can be due to rapid changes in river flow over short time scales, during which the river does not come to equilibrium with the changing flows (Hoyt and Grover 1912; Westphal et al. 1999), interactions between the main channel and the floodplain (Ackers 1993), and transitions between early and late regime flows and associated changes in bed forms (Westphal et al. 1999; Paarlberg et al. 2010). Hysteresis effects in the Mississippi River are especially prevalent at medium to high flow conditions (greater than 15,000 $m^3 s^{-1}$) at upstream locations such as Baton Rouge, Louisiana; Donaldsonville, Louisiana; and to a lesser extent, New Orleans. There is an especially high correlation at these stations between the time rate of change in flow and the deviation from the mean flow stage curve. During rapid increases in daily flows, water levels at Baton Rouge, Louisiana, can be 1 m lower than the mean water levels for steady-state flow conditions, while for rapid decreases in flows, water levels increase by as much as 75 cm.

The form of the flow stage curves shows pronounced leveling off of stages as flows increase beyond 22,000 $m^3 s^{-1}$, indicating increased efficiency of the river at high flows related to the degradation of riverbed ripples and dunes that reduces frictional resistance, and increased lateral discharge in the lower reaches of the river. These processes are now reflected in the model through the regime-dependent variation in bottom friction as well as the improved representation of the east river bank. In the lower river, there is no eastern artificial levee south of Pointe à la Hache, Louisiana; rather, a low natural levee on the east bank extends south to Venice, Louisiana, allowing high river discharge to spill into adjacent marshes and bays. Riverine flow for the range of stages is entirely constrained within the levees upriver of Pointe à la Hache, Louisiana; south of Pointe à la Hache to Venice, Louisiana, the river is mostly contained up to 20,000 $m^3 s^{-1}$; higher flows overtop the low eastern river bank into many bays in Caernarvon Marsh, and passes such as Baptiste Collette allow flow to exit directly into Breton Sound. Thus, along the progression of the lower river toward the ocean outlets, flow and frictional resistance decrease, leading to lower slopes in the flow stage curves of downriver gauges such as Empire, Louisiana, and Venice, Louisiana.

Flow stage relationships for the SL16 model, without and with the regime-based bottom friction, are compared to the best-fit measurement data curves at the various river stations in Fig. 3. These simulations applied steady river flows at Baton Rouge, Louisiana, were performed without tides, used the north-central Gulf annual mean sea level, and in all cases achieved a steady state. The SL16 flow stage curves are therefore expected to fall within the central portion of the measurement data scatter. The computed and measured flow rates in Fig. 3 are limited to not exceed 32,000 $m^3 s^{-1}$, which is the flow rate at which the USACE opens the Bonnet Carre and other spillways. The SL16 model without regime-based friction overpredicts the flow stage curves at high flows at upriver stations, while the SL16 model with regime-based friction more closely matches the data for all flow rates and at all stations. Considering regime-dependent friction reduces water levels at Baton Rouge, Louisiana, and Donaldsonville, Louisiana, by up to 1 m at flows above 30,000 $m^3 s^{-1}$, and water levels at New Orleans and Alliance reduce by 10–20 cm. It is noted that gauges south of Alliance are unaffected by the use of a regime-dependent friction. This is due to low slopes at downriver gauges such as Empire, Louisiana, and Venice, Louisiana, which maintain low depth-averaged velocities and do not approach transitional or high regimes.

Table 1 summarizes the average absolute errors in the SL16 model stages without and with the regime-based variation in bottom friction as compared to the measurement-derived best-fit curves, and the average absolute errors between the measurement data points as compared to the measurement-derived best-fit curves. Using the regime-dependent bottom friction, errors between the SL16 computed stages and the measurement-derived best-fit curve are significantly improved. Errors for the improved SL16 model were reduced along the length of the river, particularly at upstream locations such as Baton Rouge, Louisiana, and Donaldsonville, Louisiana. Specifically, the SL16 model with the regime-based friction has a six-station average error in the flow-stage relationship of 14 cm as compared to a 26 cm error with constant Manning's n values.

Flow Distribution through the River Distributary System

Flow distribution through passes in the river delta is another means by which to validate the model's ability to describe the flow processes of the Mississippi River. USACE Acoustic Doppler Current Profiler (ADCP)–based flow measurements are available at river and distributary cross sections at stations indicated in Fig. 1(b). When these measured distributary or river section flows are plotted as functions of the flow at Tarbert Landing, Mississippi, the scatter in the data reflects the daily and seasonal variability of the river's hydrodynamic conditions. Comparisons of linear and quadratic best-fit curves of the flow at Tarbert Landing, Mississippi, versus the distributary or river section flow show that a quadratic fit curve is a closer representation of the measured flows. Table 2 shows the flows and the percentage flows relative to Tarbert Landing, Mississippi, obtained at the various sections/distributaries for both the model and the measured data over a range of riverine discharges. Flow is mostly contained within the river from low to high flows; however, there is increasing lateral leakage south of Pointe à la Hache, Louisiana, as river flows increase. There is a moderate redistribution of flows throughout the various passes as flow increases; however, total flows within these passes increase with increasing riverine discharges. Generally approximately 10% of the river's flow exits through both Baptiste Collette and Grand Pass, and approximately half of the river's flow exits prior to the river approaching Pilot's Town. One-third of river flow exits through Southwest Pass, and 10% exits through both South Pass and Pass a Loutre.

ADCIRC-computed flows at these locations are also shown in Table 2. In general, the comparisons between ADCIRC and the measured data quadratic fit percentages are good, with an overall best-fit slope of 0.99 and an R^2 value of 0.93. In almost all cases, ADCIRC-computed flows and percentages are at or near the quadratic fit estimates. The comparisons indicate that the model underpredicts flows through Pass a Loutre, and overpredicts flows through Grand Pass. Overall, the ADCIRC model and SL16 mesh with flow regime–based friction replicate the river flow stages and the flow distribution through the distributary system very well.

Hurrican Gustav Validation

Hurricane Gustav (2008) has been validated on the SL16 mesh in previous work (Dietrich et al. 2011a, 2012) through comparison to

J. Hydraul. Eng. 2013.139:492-501.

Table 2. Flow Distribution through Mississippi River Distributaries for Three Riverine Discharges at Tarbert Landing, Mississippi

	Station	ADCIRC m^3/s	ADCIRC %	Measured m^3/s	Measured %
13,420 $m^3\,s^{-1}$	Pointe à la Hache, Louisiana	13,420	100		
	Venice, Louisiana	10,830	81		
	Baptiste Collette	1,696	13	1,341	10
	Grand Pass	2,153	16	1,314	10
	Cubits Gap, Louisiana	1,041	8	1,611	12
	Pilots Town	7,440	55	7,307	54
	Southwest Pass	5,451	41	4,396	33
	South Pass	1,394	10	1,488	11
	Pass a Loutre	568	4	1,430	11
22,670 $m^3\,s^{-1}$	Pointe à la Hache, Louisiana	22,674	100		
	Venice, Louisiana	16,414	72		
	Baptiste Collette	2,749	12	1,974	9
	Grand Pass	3,440	15	2,064	9
	Cubits Gap, Louisiana	2,008	9	2,379	10
	Pilots Town	10,810	48	11,595	51
	Southwest Pass	7,792	34	7,440	33
	South Pass	1,779	8	2,171	10
	Pass a Loutre	1,130	5	2,044	9
31,710 $m^3\,s^{-1}$	Pointe à la Hache, Louisiana	31,712	100		
	Venice, Louisiana	19,293	61		
	Baptiste Collette	3,243	10	2,558	8
	Grand Pass	3,972	13	2,553	8
	Cubits Gap, Louisiana	2,471	8	3,039	10
	Pilots Town	12,445	39	14,096	44
	Southwest Pass	8,871	28	8,934	28
	South Pass	1,997	6	2,837	9
	Pass a Loutre	1,404	4	2,537	8

Note: Measured flow data are based on quadratic best-fit curves of the flow at Tarbert Landing, Mississippi, versus the flow through specific distributaries or river sections provided by the USACE. ADCIRC flow values are based on the SL16 model with flow regime based friction.

high water marks and wave and water elevation time-history gauge data throughout the region. In this paper, the SL16 model is applied with the river velocity regime–dependent Manning's n and the temporally varying flow-driven river radiation boundary condition, and the focus is the Mississippi River response. The effect of waves on storm surge generation is considered and combined wind, atmospheric pressure, wave, and tide-driven water levels are simulated. SWAN + ADCIRC–generated water elevations are compared to NOAA and USACE hydrographs where available at various locations along the river. Riverine and tidal forcing are specified in "ADCIRC Model and the River Radiation Boundary Condition." Riverine and tidal spin-up times for Gustav are summarized in Dietrich et al. (2011a). Riverine flows during Gustav ranged from 8,000 m^3s^{-1} at Gustav's landfall to 11,500 m^3s^{-1} 4 days after the storm's passage through southern Louisiana.

Wind fields for Gustav are data-assimilated using NOAA's Hurricane Research Division Wind Analysis System (H*WIND) for the inner core (Powell et al. 1996, 1998), and the Interactive Objective Kinematic Analysis (IOKA) system for Gulf-scale winds (Cox et al. 1995; Cardone and Cox 2007). These winds represent the most detailed and accurate time and space–dependent history of the hurricane; the synoptic history is described and illustrated by Dietrich et al. (2011a).

Gustav made landfall early on September 1, 2008, at Terrebonne Bay, Louisiana, approximately 75 km to the southwest of New Orleans. The storm entered the Gulf and approached southwestern Louisiana as a Category 3 storm on the Saffir-Simpson scale, but weakened to a Category 1 storm as it made landfall (Beven and Kimberlain 2009; Forbes et al. 2010; Dietrich et al. 2011a). Although Gustav was a less-intense storm than Katrina, it was considerably larger, with tropical storm–force winds extending 350 km from the storm's center. The storm tracked west of the Mississippi River delta, but its size allowed easterly and southeasterly tropical storm–force winds to blow across the Mississippi–Alabama (MS-AL) continental shelf for more than 24 h prior to landfall. Compared to previous storms, more data were available for validation of Gustav due to deployment of new gauges and hardening of existing gauges that had failed during Katrina. Accordingly, there was a substantial increase in recorded measurements within the Mississippi River prior to and during the storm. Measured water levels at USACE-maintained gages were compared to SWAN + ADCIRC–generated water levels at nine locations within the Mississippi River (Fig. 4).

Prior to landfall, strong winds pushed water across the MS-AL shelf, causing maximum water level buildups of 2–3 m against the levees of lower Plaquemines Parish, Louisiana. Surge from Breton Sound entered the river south of Pointe à la Hache, Louisiana, built against the western river levee, and propagated upriver. Surge south of USACE gauge 01480 at Venice, Louisiana, and in the delta was modest, with peak water levels of 1.5 m recorded at NOAA gauge 8760922 at Southwest Pass and 2.0 m at USACE gauge 01545 at Head of Passes, respectively. Surge north of Venice, Louisiana, was contained against the western levee and led to increased water levels up to 3 m. This surge propagated upriver, leading to peak water elevations of more than 3 m at USACE gauge 01300 in New Orleans. In the upper reaches of the river, water elevations prior to the storm surge passage decreased due to a decrease in riverine flow from 9,250 to 7,930 m^3s^{-1}. This effect is seen at USACE gauge 01220 at Donaldsonville, Louisiana, USACE gauge 01260 at Reserve, Louisiana, and to a lesser extent at USACE gauge 01275 at the Bonnet Carre Spillway north of Carrollton, Louisiana, where elevations decreased by as much as 0.5 m due to the river flow reduction. River stages returned to ambient levels approximately 1.5 days after the storm had passed, and upriver gauges indicate increases in water levels due to rising river flows.

SWAN + ADCIRC–predicted elevations compare well to measured elevations along the Mississippi River during Gustav. Results from SL16 without the time-varying river flow radiation boundary condition as well as the results with this improved boundary condition are shown in Fig. 4. In particular, there has been a marked improvement in the estimation of upriver elevations prior to the main surge, where computed results accurately depict the decrease in water elevations prior to the storm's landfall, as well as peak surge. This improvement, as compared to Dietrich et al. (2011a), is due to the implementation of the time-varying river flow radiation boundary condition. Model errors of the measured time series are quantified through scatter index (SI) and bias indices (Hanson et al. 2009) as follows:

$$\mathrm{SI} = \frac{\frac{1}{N}\sqrt{\sum_{i=1}^{N}(E_i - \bar{E})^2}}{\frac{1}{N}\sum_{i=1}^{N}|O_i|} \qquad \mathrm{Bias} = \frac{\frac{1}{N}\sum_{i=1}^{N}E_i}{\frac{1}{N}\sum_{i=1}^{N}|O_i|}$$

where N = number of observations; $E_i = S_i - O_i$ is the difference between the modeled (S_i) and observed (O_i) values; and $\bar{E}$ = mean error. The SI, which indicates the ratio of the standard deviation of the measured-to-simulated errors to the mean measurements, is improved from 0.1662 for the SL16 model using a constant river flux to 0.1429 using the new SL16 model with the time-varying river flow radiation boundary condition. Bias has improved substantially, from 0.1096 in previous model efforts to 0.0202 using the current model.

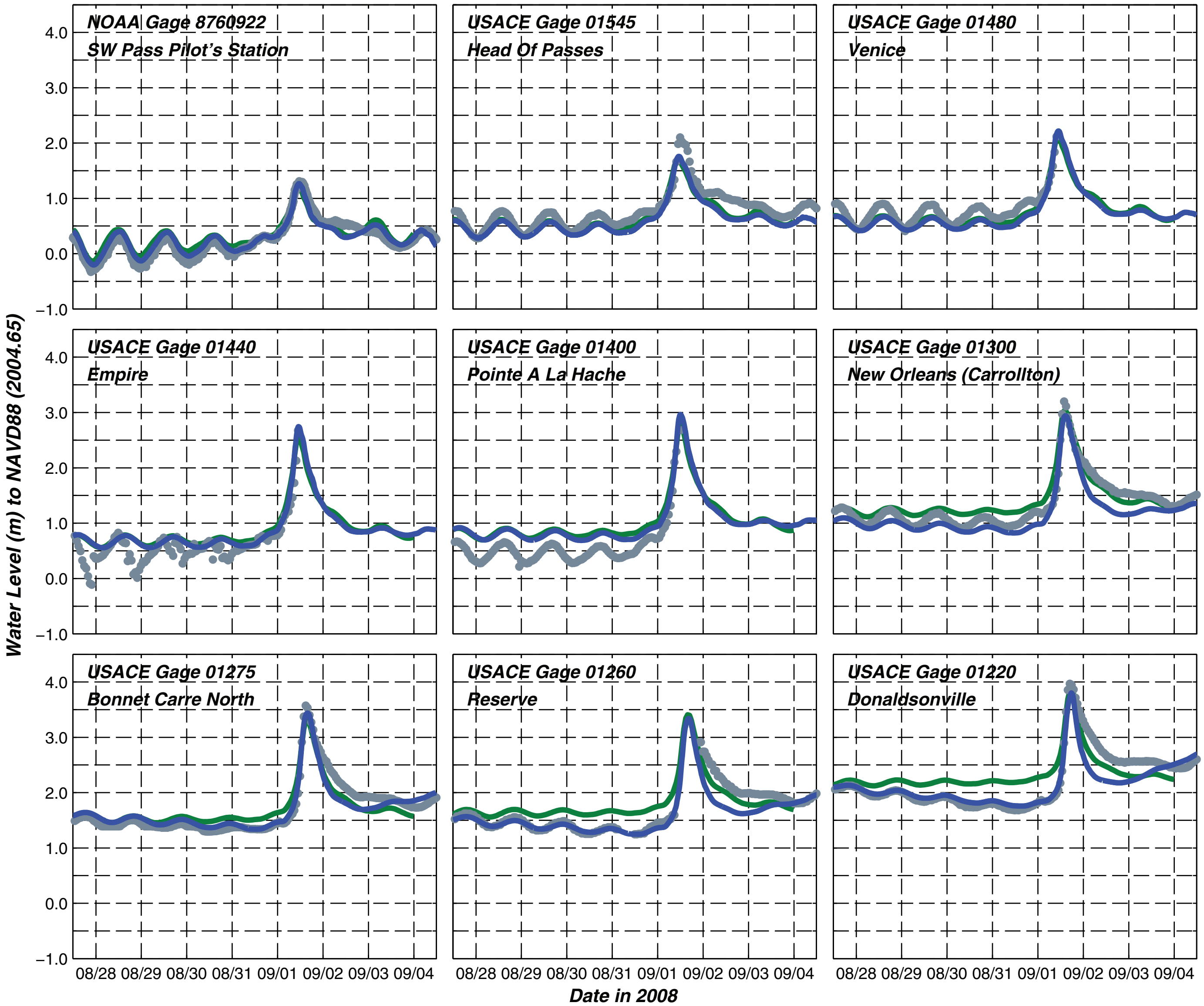

Fig. 4. (Color) Comparison of SWAN + ADCIRC–computed elevations at NOAA and USACE gauges (both shown with gray dots) along the Mississippi River during Hurricane Gustav; this paper's SL16 model results using the time-varying river radiation boundary condition are shown with blue lines; previous SL16 model using a constant river flow radiation boundary condition from Dietrich et al. (2011b) is shown with green lines

Fig. 4 shows that the time-varying river flow radiation boundary condition simulates well the falling river prior to the arrival of the storm surge as well as the rising limb of the storm surge. The falling limb of the surge appears to be better modeled with the constant river flow radiation boundary condition. The source of this error was determined to be related to the river flow measurements at Tarbert Landing, Mississippi, which in fact include the upriver flow component associated with the storm surge itself, i.e., the flow measurements taken by the U.S. Army Corps of Engineers are the total river flow and do not parse out the river-only component and the component of surge. Simulations with the SL16 model that increase the specified river flow at Baton Rouge, Louisiana, from September 1 to 3, 2008, the time that the surge passed Tarbert Landing, Mississippi, indicate that the recession portion of the river surge is much better modeled. However, because Tarbert Landing, Mississippi, is not included in the model, it is not possible to estimate the increase in the river-only flow that is used as a component of the radiation boundary condition. The tidal signal prior to the storm and the evolution of water levels during the storm are generally well predicted, though there is some attenuation in the tidal amplitudes, as seen in USACE gauges 01400, 01440, and 01480. The model may be missing an efficient connection to open Gulf waters that effectively amplifies tides in this portion of the river.

Conclusions

The recently developed, unstructured mesh SL16, SWAN + ADCIRC wave-circulation model simulates riverine flows, tides, and hurricane waves and circulation for southeastern Louisiana and the Mississippi River. Increased resolution in the SL16 model of the river, its delta, and surrounding wetlands (Dietrich et al. 2011a), along with an improved parameterization of frictional resistance and a time-dependent river flow radiation boundary condition presented in this paper provide the ability to accurately model riverine flows, hurricane storm surges, and their interaction in this geographically complex river and delta environment.

J. Hydraul. Eng. 2013.139:492-501.

The SL16 model has increased mesh resolution in the river, its banks, and batture, and includes more channels and passes, as well as land use–derived topography for the surrounding wetlands as compared with the earlier SL15 model. Model refinements in this paper include the use of a regime-based dependence in bottom friction associated with the degradation of riverbed ripples and dunes for high river velocities. This is shown to reduce high river flow water levels at the upriver stations and improve the flow stage relationships. The SL16 model with the regime-dependent Manning's n friction relationship produces a mean 14-cm station average absolute error between the model and the best-fit measurement data flow stage curves. In addition, the refined SL16 model simulates well the distribution of flows within the distributary system in the lower river. Quadratic fit estimates of measured river flow indicate that the model accurately represents flows through the river distributaries and deltaic channels, with a best-fit slope near unity and a correlation coefficient R^2 value of 0.93.

The development of a time-varying riverine flow radiation boundary condition adds the ability to model falling and rising river flow–based water levels during a hurricane event. Comparisons to NOAA and USACE hydrographs along the Mississippi River show that the improved SWAN + ADCIRC SL16–modeled water levels depict well the evolution of water elevations during Hurricane Gustav, when large fluctuations in river discharge cause up to a 50 cm change in ambient water levels. Model performance is quantified through scatter index and bias for the SL16 model with constant and time-varying river flow radiation boundary conditions. Model performance was improved through the implementation of a temporally varying riverine flow-driven radiation boundary condition, allowing the model to capture the time variations in river flow. The SI is improved from 0.1662 for the SL16 model using a constant river flow to 0.1429 using the temporally varying riverine flow boundary condition and bias has improved substantially, from 0.1096 to 0.0202.

Appendix. Geographic Locations by Number Shown in Fig. 1

1. Mississippi River
2. Chandeleur Sound
3. Breton Sound
4. Lake Borgne
5. Lake Pontchartrain
6. Barataria Bay
7. Terrebonne Bay
8. Chandeleur Islands
9. Louisiana-Mississippi Shelf
10. Biloxi marsh
11. Caernarvon marsh
12. Plaquemines Parish, Louisiana
13. USACE gauge 01160 at Baton Rouge, Louisiana
14. USACE gauge 01220 at Donaldsonville, Louisiana
15. USACE gauge 01260 at Reserve, Louisiana
16. USACE gauge 01275 at Bonnet Carre—Above lock
17. USACE gauge 01300 at Carrollton New Orleans
18. USACE gauge 01390 at Alliance
19. USACE gauge 01400 at West Pointe à la Hache, Louisiana
20. USACE gauge 01440 at Empire, Louisiana
21. NOAA gauge 8761724 at Grand Isle, Louisiana
22. USACE gauge 01480 at Venice, Louisiana
23. USACE gauge 01545 at Head of Passes
24. Southwest Pass
25. Baptiste Collette
26. Grand Pass
27. Cubit's Gap
28. Pilot's Town
29. South Pass
30. Pass a Loutre
31. NOAA gage 8760922 at Southwest Pass Pilot's Station.

Acknowledgments

This work was supported by the United States Army Corps of Engineers (USACE) New Orleans District (MVN) and the USACE System-Wide Water Resources and Morphos Programs. Computational resources and support were provided by the University of Texas at Austin Texas Advanced Computing Center (TACC). Permission to publish this paper was granted by the Chief of Engineers, USACE.

References

Ackers, P. (1993). "Stage-discharge functions for two-stage channels: The impact of new research." *J. Inst. Water Environ. Manage.*, 7(1), 52–61.

American Congress on Surveying and Mapping. (1992). Surveying and land information systems, Vol. 52, *No. 3*, 133–149, ⟨http://www.ngs.noaa.gov/PUBS_LIB/NAVD88/navd88report.htm⟩.

Arcement, G. J., and Schneider, V. R. (1989). "Guide for selecting Manning's roughness coefficients for natural channels and flood plains." *United States Geological Survey Water Supply Paper 2339*, U.S. Government Printing Office, Washington, DC.

Atkinson, J. H., Westerink, J. J., and Hervouet, J. M. (2004a). "Similarities between the quasi-bubble and the generalized wave continuity equation solutions to the shallow water equations." *Int. J. Numer. Methods Fluids*, 45(7), 689–714.

Atkinson, J. H., Westerink, J. J., and Luettich, R. A. (2004b). "Two-dimensional dispersion analysis of finite element approximations to the shallow water equations." *Int. J. Numer. Methods Fluids*, 45(7), 715–749.

Beven, J. L., II, and Kimberlain, T. (2009). "Tropical cyclone report, Hurricane Gustav (AL072008), 25 August–4 September, 2008." National Hurricane Center, National Oceanographic and Atmospheric Administration, Washington, DC.

Booij, N., Ris, R. C., and Holthuijsen, L. (1999). "A third-generation wave model for coastal regions, part 1, model description and validation." *J. Geophys. Res.*, 104(C4), 7649–7666.

Buczkowski, B. J., Reid, J. A., Jenkins, C. J., Reid, J. M., Williams, S. J., and Flocks, J. G. (2006). "usSEABED: Gulf of Mexico and Caribbean (Puerto Rico and U.S. Virgin Islands) offshore surficial sediment data release." U.S. Geological Survey Data Series 146, Version 1.0, ⟨http://pubs.usgs.gov/ds/2006/146/⟩ (Feb. 5, 2013).

Bunya, S., et al. (2010). "A high resolution coupled riverine flow, tide, wind, wind wave and storm surge model for southern Louisiana and Mississippi: Part I Model development and validation." *Mon. Weather Rev.*, 138(2), 345–377.

Cardone, V. J., and Cox, A. T. (2007). "Tropical cyclone wind field forcing for surge models: Critical issues and sensitivities." *Nat. Hazards*, 51(1), 29–47.

Chow, V. T. (1959). *Open channel hydraulics*, McGraw-Hill, New York.

Cox, A. T., Greenwood, J. A., Cardone, V. J., and Swail, V. R. (1995). "An interactive objective kinematic analysis system." *Proc., 4th Int. Workshop on Wave Hindcasting and Forecasting*, Atmospheric Environment Service, Banff, Alberta, Canada, 109–118.

Dawson, C., Westerink, J. J., Feyen, J. C., and Pothina, D. (2006). "Continuous, discontinuous, and coupled discontinuous-continuous Galerkin finite element methods for the shallow water equations." *Int. J. Numer. Methods Fluids*, 52(1), 63–88.

Dietrich, J. C., et al. (2010). "A high resolution coupled riverine flow, tide, wind, wind wave and storm surge model for southern Louisiana and

J. Hydraul. Eng. 2013.139:492-501.

Mississippi: Part II—Synoptic description and analyses of Hurricanes Katrina and Rita." *Mon. Weather Rev.*, 138(2), 378–404.

Dietrich, J. C., et al. (2011a). "Hurricane Gustav (2008) waves and storm surge: Hindcast, synoptic analysis and validation in southern Louisiana." *Mon. Weather Rev.*, 139(8), 2488–2522.

Dietrich, J. C., et al. (2011b). "Modeling hurricane waves and storm surge using integrally-coupled, scalable computations." *Coastal Eng.*, 58(1), 45–65.

Dietrich, J. C., et al. (2012). "Performance of the unstructured-mesh, SWAN+ADCIRC model in computing hurricane waves and surge." *J. Sci. Comput.*, 52(2), 468–497.

Egbert, G. D., and Erofeeva, S. Y. (2002). "Efficient inverse modeling of barotropic ocean tides." *J. Atmos. Oceanic Techno.*, 19(2), 183–204.

Forbes, C., Luettich, R. A., Mattocks, C. A., and Westerink, J. J. (2010). "A retrospective evaluation of the storm surge produced by Hurricane Gustav (2008): Forecast and hindcast results." *Weather Forecast.*, 25(6), 1577–1602.

Hanson, J. L., Tracy, B. A., Tolman, H. L., and Scott, R. D. (2009). "Pacific hindcast performance of three numerical wave models." *J. Atmos. Oceanic Technol.*, 26(8), 1614–1633.

Hoyt, J., and Grover, N. C. (1912). *River discharge*, 2nd Ed., Wiley, New York.

Kubatko, E. J., Bunya, S., Dawson, C., Westerink, J. J., and Mirabito, C. (2009). "A performance comparison of continuous and discontinuous finite element shallow water models." *J. Sci. Comput.*, 40(1–3), 315–339.

Le Provost, C., Lyard, F., Molines, J. M., Genco, M. L., and Rabilloud, F. (1998). "A hydrodynamic ocean tide model improved by satellite altimeter-derived data set." *J. Geophys. Res.*, 103(C3), 5513–5529.

Luettich, R. A., and Westerink, J. J. (2004). "Formulation and numerical implementation of 2D/3D ADCIRC finite element model version 44.XX." ⟨http://www.adcirc.org/adcirc_theory_2004_12_08.pdf⟩ (Feb. 5, 2013).

Mukai, A., Westerink, J. J., Luettich, R. A., and Mark, D. J. (2001). "Guidelines for using the East Coast 2001 database of tidal constituents within the western North Atlantic Ocean, Gulf of Mexico and Caribbean Sea." *Coastal and Hydraulic Engineering Technical Note*, U.S. Army Engineer Research and Development Center, Vicksburg, MS.

Paarlberg, A., Dohmen-Janssen, C. M., Hulsher, S. J. M. H., Termes, P., and Schielen, R. (2010). "Modeling the effect of time-dependent river dune evolution on bed roughness and stage." *Earth Surf. Processes Landforms*, 35(15), 1854–1866.

Powell, M. D., Houston, S., Amat, L., and Morrisseau-Leroy, N. (1998). "The HRD real-time hurricane wind analysis system." *J. Wind Eng. Ind. Aerodyn.*, 77–78(1), 53–64.

Powell, M. D., Houston, S., and Reinhold, T. (1996). "Hurricane Andrew's landfall in South Florida. Part I: Standardizing measurements for documentation of surface wind fields." *Weather Forecast.*, 11(3), 304–328.

Resio, D. T., and Westerink, J. J. (2008). "Modeling the physics of storm surges." *Phys. Today*, 61(9), 33–38.

Ris, R. C., and Holthuijsen, L. H. (1999). "Spectral modelling of current induced wave-blocking." *Proc., 25th Int. Conf. on Coastal Engineering*, ASCE, New York, 1247–1254.

Sanchez-Rubio, G., Perry, H. M., Biesot, P. M., Johnson, D. R., and Lipcius, R. N. (2011). "Oceanic-atmospheric modes of variability and their influence on riverine input to coastal Louisiana and Mississippi." *J. Hydrol.*, 396(1–2), 72–81.

Tanaka, S., Bunya, S., Westerink, J. J., Dawson, C., and Luettich, R. A. (2011). "Scalability of an unstructured grid continuous Galerkin based hurricane storm surge model." *J. Sci. Comput.*, 46(3), 329–358.

van Rijn, L. C. (2007). "Unified view of sediment transport by currents and waves. III: Graded beds." *J. Hydraul. Eng.*,133(7), 761–775.

Walker, N. D., Wiseman, W. J., Jr., Rouse, L. J., Jr., and Babin, A. (2005). "Effects of river discharge, wind stress, and slope eddies on circulation and the satellite-observed structure of the Mississippi River plume." *J. Coastal Res.*, 21(6), 1228–1244.

Warner, J. C., Sherwood, C. R., Signell, R. P., Harris, C. K., and Arango, H. G. (2008). "Development of a three-dimensional, regional, coupled wave, current, and sediment-transport model." *Comput. Geosci.*, 34(10), 1284–1306.

Westerink, J. J., et al. (2008). "A basin to channel scale unstructured grid hurricane storm surge model applied to southern Louisiana." *Mon. Weather Rev.*, 136(3), 833–864.

Westphal, J., Thompson, D. B., Stevens, G. T., and Strauser, C. N. (1999). "Stage-discharge relationships on the middle Mississippi River." *J. Water Resour. Plann. Manage.*, 125(1), 48–53.

Zijlema, M. (2010). "Computation of wind-wave spectra in coastal waters with SWAN on unstructured grids." *Coastal Eng.*, 57(3), 267–277.